3rd URSI AT-AP-RASC, Gran Canaria, 29 May – 3 June 2022

Thermographic image super-resolution based on neural networks

A. Galván-Hernández [(1)], J. R. Ticay-Rivas [(1)], V. Alonso-Eugenio[(1)], V. Araña[(1)] and F. Cabrera[(1)]
(1) IDeTIC, Universidad de Las Palmas de Gran Canaria, https://www.ulpgc.es/

Abstract

The continuous development of thermographic technology has led to the overall improvement of instruments used in medicine, surveillance, or military systems. However, thermographic imaging cameras still have a high cost compared to other alternatives on the market, such as visible light cameras and a much lower spatial resolution. Super-resolution is a technique that improves the visual quality of an image through software processing. This work studies three neural networks architectures based on deep learning capable of performing super-resolution of RGB images at x2 and x4 scales: Photo-Realistic Single Image Super-Resolution Using a Generative Adversarial Network (SRGAN), Enhanced Deep Residual Networks for Single Image Super-Resolution (EDSR), and Wide Activation for Efficient and Accurate Image Super-Resolution (WDSR). These architectures, in this work, have been trained as a super-resolution system using thermographic images as input data. The evaluation was carried out using thermographic images from different thermographic cameras. The performance assessment was carried out using the Peak Signal to Noise Ratio (PSNR) and the Structural Similarity Index Measure (SSIM). In addition, low-resolution images from a low-cost thermographic camera were used as input to the neural networks to study the feasibility of this method.

1 Introduction

Thermographic technology is used in a wide range of applications in fields such as astrophysics, medicine, materials science, chemistry, meteorology, and military systems, among others [1]. A thermographic camera detects the thermal radiation from a scene by concentrating it on a sensor to produce a physical effect. More than 95% of thermographic camera sensors are microbolometers [2] since they do not require active cooling and their reduced size.

Given the complexity of the manufacturing processes for microbolometer arrays and the relatively low demand for these systems, the price of thermographic cameras is generally high [1, 2]. In addition, despite the current technological innovation in thermography, the most standard available resolutions are 640x480, 320x240, and 160x120 [3, 4].

A novel approach to improve the spatial resolution of these cameras is to apply super-resolution (SR) techniques. These techniques aim to increase the level of pixels and details that characterize an image, increasing the visual quality of the image [5]. However, from a practical point of view, SR techniques have been limited by computing power [6].

This technique has been developed and implemented for images generated in the visible range. Recently, different approaches to this technique have been made to the field of thermography. On the one hand, Więcek et al. proposed a residual neural network (NN) with a reduced number of layers using a transfer learning strategy through RGB images [7]. On the other hand, V. Chudasama et al. proposed a NN for thermographic images with better computational efficiency compared to other state-of-the-art techniques [8]. Finally, P. Cascarano et al. proposed a NN architecture that introduces different regularization terms to improve training efficiency, in addition to an automated choice of network parameters without the need for a priori knowledge of the training dataset used [9].

This work proposes to use three new NN architectures for thermal SR: Photo-Realistic Single Image Super-Resolution Using a Generative Adversarial Network (SRGAN) [10], Enhanced Deep Residual Networks for Single Image Super-Resolution (EDSR) [11] and Wide Activation for Efficient and Accurate Image Super-Resolution (WDSR) [12]. To evaluate their performance, we have created a thermal dataset and used the Peak Signal to Noise Ratio (PSNR) and the Structural Similarity Index Measure (SSIM) as performance metrics, which are widely used to evaluate the different SR techniques in the state of the art [5, 6].

The remainder of this paper is organized as follows: Section 2 describes the database and the thermographic cameras used in the experiments. Section 3 describes the types of NN-based architectures used. Section 4 details the experiments and the results obtained. Finally, the conclusions derived from the results are presented in Section 5.

2 Materials

Two datasets of thermographic images were used in this work. The first one is the “ADAS” dataset provided by the thermographic imaging camera manufacturer FLIR [13]. This dataset has 10228 images divided into 8862 training

images and 1366 validation images. The formats available are: RGB format (1800x1200), 8-bit thermographic format (640x512) and 16-bit thermographic format (640x512).

The second dataset was generated from three different thermographic cameras, named Database for the Assessment of Spatial Super-Resolution (DASSR), and has 160 thermographic images per camera from different measurement scenarios. Figure 1 illustrates the integration of these cameras. The general characteristics of the cameras used are described in Table 1.

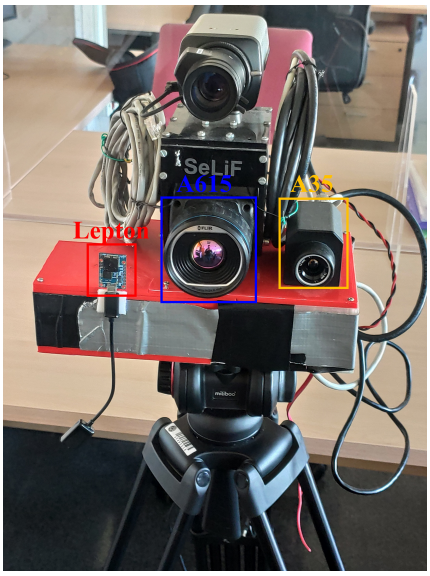

Figure 1. FLIR cameras used for the creation of the DASSR dataset

Table 1. General characteristics of the cameras used

	General characteristics			
Cameras	**Resolution**	**Focal length (mm)**	**HFOV (°)**	**VFOV (°)**
FLIR A615	640 x 480	24.6	25	18.8
FLIR A35	320 x 256	19	24	19.2
FLIR Lepton	160 x 120	2	57	42

3 Architectures for thermal super-resolution

The super-resolution NN architectures have a learning model capable of mapping the relationship between a low-resolution (LR) image and its high-resolution (HR) equivalent through a specific training and evaluation process.

In this work three different SR architectures have been implemented: the NN architecture presented in "Photo-Realistic Single Image Super-Resolution Using a Generative Adversarial Network" [10], the NN architecture presented in "Enhanced Deep Residual Networks for Single Image Super-Resolution" [11] and the NN architecture presented in "Wide Activation for Efficient and Accurate Image Super-Resolution" [12]. All details corresponding to the number of layers and the learning strategy designed by the respective authors can be found in the original articles [10, 11, 12].

3.1 SRGAN

The architecture proposed in SRGAN is based on using Generative Adversarial Networks (GAN). In this type of network, a generator is responsible for creating an SR image from an LR image and a discriminator responsible for verifying whether the SR image is similar to the original image. The confrontation between these two networks allows the generator to learn how to create an SR image. Furthermore, the same premise is used during the training phase, achieving a series of results not seen before the implementation of GAN networks.

3.2 EDSR

The EDSR architecture uses the innovations made by SRGAN but without using a GAN network. Instead, this NN uses a residual block called SRResNET, which is very present in the learning process when extracting features in an image. EDSR leverages and adapts SRResNET by eliminating batch normalization, which improves the training process concerning other NN architectures.

3.3 WDSR

The WDSR architecture uses the changes established by EDSR, eliminating batch normalization in the training stage. In addition, introduce a feature expansion using convolutional layers before reaching the ReLu activation function. This modification allows more information to pass through while maintaining the high nonlinearity of deep NN. In this work, the WDSR-B architecture proposed by the authors has been studied.

4 Experiments and results

The implementation of the NN architectures found in [14] for SRGAN and the implementation found in [15] for EDSR and WDSR-B have been used. Training and validation were performed using the ADAS dataset, specifically the images in 8-bit format. Finally, to evaluate the final performance, the DASSR dataset was used.

The performance metrics are PSNR defined as:

$$\mathrm{PSNR} = 10 \cdot \log_{10}\left(\frac{L^2}{\frac{1}{N}\sum_{i=1}^{N}(I-\hat{I})^2}\right) \tag{1}$$

Where L is equal to 255 in the general cases using 8-bit representations and 65535 in 16-bit representations, I is the original image and $\hat{I}$ is the processed image.

The SSIM is defined as:

$$\mathrm{SSIM}(I,\hat{I}) = \frac{(2\mu_I\mu_{\hat{I}}+C_1)(\sigma_{I\hat{I}}+C_2)}{\left(\mu_I^2+\mu_{\hat{I}}^2+C_1\right)\left(\sigma_I^2+\sigma_{\hat{I}}^2+C_2\right)} \tag{2}$$

Where μ_x represents the image mean, σ_x represents the image standard deviation, $\sigma_{I\hat{I}}$ represents the covariance between two images and C_1, C_2 are constants set to avoid instability.

In order to apply the proposed SR architectures to the thermographic images of the DASSR dataset, it has been necessary to convert the 16-bit thermographic images into 8-bit images (normalization), storing reference data that are equivalent to the object temperature. Then, after applying the SR, these references are used to return to the 16-bit range (denormalization).

The DASSR dataset has been segmented into 4 sets: DASSR-I (40 images), DASSR-II (60 images), DASSR-III (30 images) and DASSR-IV (30 images). The images found in each of these sets present similar scenarios, so the results obtained from PSNR and SSIM will be an average of all these images providing the standard deviation of each set.

Two experiments are proposed from this dataset. The first one consists of using the A615 camera samples of each subset. The LR images were generated through a bicubic interpolation, downscaling the images by a factor of x2 and x4. After applying SR on these LR images, SR images have been obtained for further comparison with the original images. It should be taken into account that the PSNR has been studied concerning a 16-bit thermographic image, so the theoretical values that can be obtained in the optimal case are close to 96 dB (PSNR = $20\log(2^{16})$). The results of this experiment can be seen in Table 2 and Table 3.

Table 2. First results with x2 scale

	SR with x2 scale			
Architecture used	**PSNR**	**SSIM**	**PSNR**	**SSIM**
SRGAN	74.85 ± 1.91	1.0 ± 0.0	79.77 ± 1.63	1.0 ± 0.0
EDSR	78.45 ± 1.66	1.0 ± 0.0	81.12 ± 0.94	1.0 ± 0.0
WDSR-B	76.79 ± 2.61	1.0 ± 0.0	80.68 ± 1.22	1.0 ± 0.0
	DASSR-I		DASSR-II	
	Set			
	DASSR-III		DASSR-IV	
SRGAN	78.28 ± 2.30	1.0 ± 0.0	65.70 ± 1.03	0.9997 ± 0.0001
EDSR	80.97 ± 1.04	1.0 ± 0.0	66.93 ± 1.25	0.9998 ± 0.0001
WDSR-B	80.30 ± 1.52	1.0 ± 0.0	66.35 ± 1.12	0.9998 ± 0.0001
Architecture used	**PSNR**	**SSIM**	**PSNR**	**SSIM**
	SR with x2 scale			

Table 3. First results with x4 scale

	SR with x4 scale			
Architecture used	**PSNR**	**SSIM**	**PSNR**	**SSIM**
SRGAN	72.43 ± 3.19	0.9999 ± 0.0	78.57 ± 1.93	1.0 ± 0.0
EDSR	72.59 ± 3.31	0.9999 ± 0.0	78.62 ± 1.8	1.0 ± 0.0
WDSR-B	72.05 ± 3.58	0.9999 ± 0.0001	78.51 ± 1.86	1.0 ± 0.0
	DASSR-I		DASSR-II	
	Set			
	DASSR-III		DASSR-IV	
SRGAN	77.30 ± 2.74	1.0 ± 0.0003	59.01 ± 1.05	0.9987 ± 0.0
EDSR	77.98 ± 2.36	1.0 ± 0.0004	58.19 ± 1.09	0.9984 ± 0.0
WDSR-B	77.90 ± 2.41	1.0 ± 0.0004	57.75 ± 1.13	0.9983 ± 0.0
Architecture used	**PSNR**	**SSIM**	**PSNR**	**SSIM**
	SR with x4 scale			

The second experiment consisted of applying SR to images from the Lepton camera. The results of this experiment, applying an x4 scaling factor, are shown in Figure 3, Figure 4 and Figure 5, where a specific sample has been extracted from the DASSR database and presented after applying the SR. In addition, the original image is shown in Figure 2. These images show the improvement in spatial resolution offered by this type of technique when applied to a low-cost thermographic imaging camera.

Figure 2. Original Lepton image

Figure 3. SRGAN results on the Lepton image

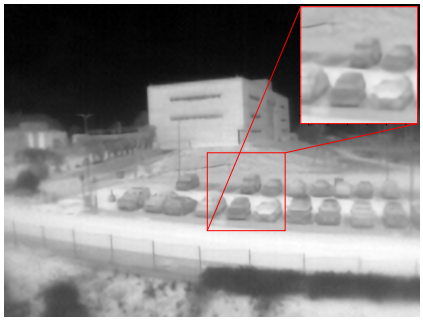

Figure 4. EDSR results on the Lepton image

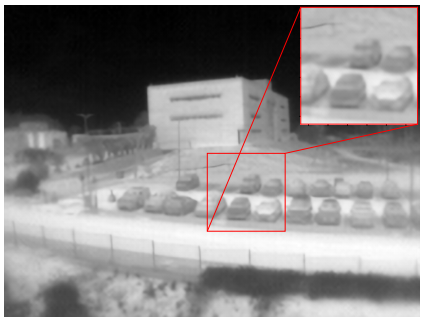

Figure 5. WDSR-B results on the Lepton image

5 Conclusions

This article presents three NN architectures capable of improving the spatial resolution of an image through deep learning. In the current state of the art, these architectures have been used to apply SR to RGB images, training and evaluating the models through datasets containing images in the visible spectrum. However, this article proposes its use for SR thermographic imaging.

During the development of the work, the NN architectures have been trained with a public dataset of 8-bit thermographic images and evaluated through a dataset generated by different thermographic cameras in realistic environments. The results show a visual perceptual improvement in the samples used to evaluate the architectures, demonstrating that it is possible to improve some of the limitations in the spatial resolution that low-cost thermographic cameras have. The objective analysis of these images has been carried out in the 16-bit range, so that raw radiometric data from the thermographic cameras have been taken into account. The PSNR and SSIM results show what loss exists in the thermographic range when applying these SR techniques. Therefore, in future work, it will be possible to study what has been the actual temperature loss when applying these techniques.

6 Acknowledgements

The authors acknowledge the work carried out by Juan Domingo Santana Urbín for their contribution during this research. This work was supported by the Spanish Government under Grant (2390/2017) Project and the Interreg Mac 2104-2020 program (MAC2/3.5b/227) Project.

References

[1] R. Gade and T. B. Moeslund, “Thermal cameras and applications: a survey,” Mach. Vis. Appl. 2013 251, vol. 25, no. 1, pp. 245–262, Nov. 2013, doi: 10.1007/S00138-013-0570-5.

[2] A. Rogalski, P. Martyniuk, and M. Kopytko, “Challenges of small-pixel infrared detectors: a review,” Reports Prog. Phys., vol. 79, no. 4, p. 46501, Mar. 2016, doi: 10.1088/0034-4885/79/4/046501.

[3] B. Stark, B. Smith and Y. Chen, "Survey of thermal infrared remote sensing for Unmanned Aerial Systems," 2014 International Conference on Unmanned Aircraft Systems (ICUAS), 2014, pp. 1294-1299, doi: 10.1109/ICUAS.2014.6842387.

[4] M. Rai, “Thermal imaging system and its real time applications: a survey,” J. Eng. Technol., vol. 62, 2018.

[5] K. Nasrollahi and T. B. Moeslund, “Super-resolution: a comprehensive survey,” Mach. Vis. Appl., vol. 25, pp. 1423–1468, 2014, doi: 10.1007/s00138-014-0623-4.

[6] L. Yue, H. Shen, J. Li, Q. Yuan, H. Zhang, and L. Zhang, “Image super-resolution: The techniques, applications, and future,” Signal Processing, vol. 128, pp. 389–408, Nov. 2016, doi: 10.1016/J.SIGPRO.2016.05.002.

[7] Więcek et al., “Low-cost, low-resolution IR system with super-resolution interpolation of thermal images for industrial applications - Measurement Automation Monitoring - Tom Vol. 64, No. 4 (2018) - BazTech - Yadda.”

[8] V. Chudasama et al., “TherISuRNet - A Computationally Efficient Thermal Image Super-Resolution Network,” in 2020 IEEE/CVF Conference on Computer Vision and Pattern Recognition Workshops (CVPRW), 2020, pp. 388–397, doi: 10.1109/CVPRW50498.2020.00051.

[9] P. Cascarano et al., “Super-Resolution of Thermal Images Using an Automatic Total Variation Based Method,” Remote Sens., vol. 12, no. 10, 2020, doi: 10.3390/rs12101642.

[10] C. Ledig et al., “Photo-Realistic Single Image Super-Resolution Using a Generative Adversarial Network,” CoRR, vol. abs/1609.0, 2016.

[11] B. Lim, S. Son, H. Kim, S. Nah, and K. M. Lee, “Enhanced Deep Residual Networks for Single Image Super-Resolution,” CoRR, vol. abs/1707.0, 2017.

[12] J. Yu et al., “Wide Activation for Efficient and Accurate Image Super-Resolution,” CoRR, vol. abs/1808.0, 2018.

[13] deep newbie, “FLIR Thermal Images Dataset | Kaggle.” [Online]. Available: https://www.kaggle.com/deepnewbie/flir-thermal-images-dataset.

[14] leftthomas, “SRGAN: A PyTorch implementation of SRGAN based on CVPR 2017 paper ‘Photo-Realistic Single Image Super-Resolution Using a Generative Adversarial Network.’” [Online]. Available: https://github.com/leftthomas/SRGAN.

[15] krasserm, “super-resolution: Tensorflow 2.x based implementation of EDSR, WDSR and SRGAN for single image super-resolution.” [Online]. Available: https://github.com/krasserm/super-resolution.